River Flow 2010 - Dittrich, Koll, Aberle & Geisenhainer (eds) - © 2010 Bundesanstalt für Wasserbau ISBN 978-3-939230-00-7

Effects of relative submergence on flow and sediment patterns around clasts

A.N. Papanicolaou, A. G. Tsakiris & C.M. Kramer
IIHR-Hydroscience and Engineering, University of Iowa, Iowa City, IA, USA

ABSTRACT: The flow patterns around isolated clasts in gravel streams are governed by the clast relative submergence, which, in turn, affect the depositional patterns of incoming sediment around the clasts. To investigate the role of relative submergence on the depositional patterns around clasts, an experimental study was conducted in a recirculating laboratory flume where an array of clasts was placed atop a well-packed bed of uniform size glass beads. Two experimental scenarios were examined, namely for high (HRS) and low (LRS) relative submergence conditions. Detailed velocity profiles and surface velocity maps around the clasts were determined via an Acoustic Doppler Velocimetry and Large Scale Particle Image Velocimetry, respectively. For the HRS runs, a stagnation region was found to develop in the wake of the clasts, whose presence was minimally detectable at the water free surface. Incoming sediment deposited within the stagnation region in the clast wake. For the LRS experimental runs, a horseshoe vortex with counter-rotating limbs was the dominant flow structure due to the clast presence, which also created distinguishable flow patterns on the water free surface. Incoming sediment accumulated at the upstream face of the clasts. The findings of this study are of paramount importance towards a mechanistic approach for the deployment of clasts for fish habitat restoration.

Keywords: Relative submergence, Clasts, Horseshoe vortex, Deposition

1 INTRODUCTION

Anthropogenic activities, such as dam removal and dredging as well as installation of hydraulic structures (e.g. levees and weirs) in mountainous streams may have detrimental effects on fish habitat. To neutralize the adverse consequences from these activities and improve fish habitat, structures collectively known as fish habitat structures are installed in such streams (Shamloo et al. 2001). These structures specifically aim to provide resting, spawning and feeding areas for fish and at the same time replicate natural rocks.

One type of fish habitat structures is large rocks or clasts (Figure 1). The deceleration of the flow around the clasts creates regions of low-speed moving water, where fish may rest and feed. At the same time, the increased turbulence in the rock wake provides fish with a sunlight cover. Further, the entrapment of -typically finer- incoming sediment in the regions around the clasts provides excellent spawning grounds for fish and adds diversity, thus improving the quality of fish habitat. In contrast, areas in the vicinity of the rocks, which undergo scour, have deeper water that fish use for eluding predating species. Therefore, the interaction of the rocks with the flow and incoming sediment is intimately related to the functionality of these rocks as fish habitat structures.

The placement of large rocks is a popular practice for the rehabilitation of fish habitat in mountainous streams, because it is a low complexity and low cost solution with minimal interference to the natural environment (Fischenich and Seal, 2000). However, to date there is a lack of a mechanistic approach for the design and placement of this type of habitat structure, which are predominantly based on empirical criteria (Saldi-Caromile et al., 2004).

Figure 1. Artificially placed rocks in a stream (from Saldi-Caromile et al., 2004).

The main difficulty in the development of such a mechanistic approach for the design and placement of the rock structures is that the interaction between the rocks and the flow and the incoming sediment remain to a large degree elusive. Very few studies have examined to date the interaction between the rocks and the surrounding flow and the incoming sediment. A significant impediment in the study of rock-flow and rock-incoming sediment interactions is that in natural mountain streams, the rocks must often operate under different flow regimes. During lower flows, the rocks typically remain partially submerged (low relative submergence-LRS), whereas at higher flows the rocks occupy the lower portion of the flow depth (high relative submergence-HRS). Under the HRS regime, flow is predominantly governed by the particle Reynolds number (Re_p), whereas at LRS regime the flow is affected by localized flow structures and becomes a function of the Froude number. More importantly, different flow structures (Figure 2) arise due to the interaction between the flow and the rocks under HRS and LRS conditions (Shamloo et al. 2001).

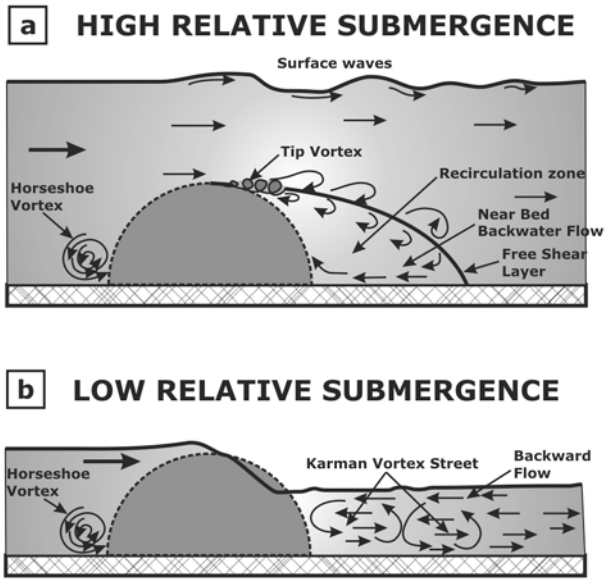

Figure 2. Vortical structures under (a) high and (b) low relative submergence conditions (after Shamloo et al. 2001).

The main objective of this research is to investigate the role of relative submergence on the sediment depositional patterns around the rocks (clasts). The specific objectives of this research are (1) to provide insight into the flow patterns around the clasts under high and low relative submergence (HRS and LRS) regimes, and (2) to associate these flow patterns with the depositional patterns of incoming sediment at high and low relative submergence regimes.

2 METHODOLOGY

2.1 *Methodological Considerations*

A series of generic experiments were conducted in order to address these objectives under conditions that are commonly encountered under field conditions.

Two experimental scenarios were investigated, namely (1) a high relative submergence scenario with H/d_c = 3.50 and (2) a low relative submergence scenario with H/d_c = 0.80, where H is the flow depth well upsteam of the clasts where their effects are minimal, and d_c is the characteristic diameter of the rocks (clasts). These H/d_c values were found in the study of Bettess (1984) to be representative of the high and low relative submergence regimes, respectively, and were kept constant throughout each experimental scenario.

For each experimental scenario a series of dimensionless bed shear stress (τ^*) levels were examined (Table 1). The dimensionless bed shear stress is calculated as:

$$\tau^* = \frac{H \cdot S}{\left(\frac{\gamma_s}{\gamma} - 1\right) \cdot d_{50}} \quad (1)$$

where d_{50} = 19.1 mm is the median diameter of the entrainable material, γ and γ_s = specific weight of the fluid and the sediment, respectively. In Table 1, Q is the volumetric flow rate, S the bed slope and $U_{bulk} = Q/(B \times H)$ the bulk velocity with B the flume width.

Table 1. Flow conditions during the experimental runs.

Test	H/d_c	τ^*	H	Q	S	U_{bulk}
	(-)	(-)	(m)	(m^3/sec)	(-)	(m/sec)
A1* 0.76	3.5	0.017	0.193	0.13	0.0024	
A2* 0.78	3.5	0.021	0.193	0.14	0.0030	
A3* 0.82	3.5	0.026	0.193	0.14	0.0036	
A4* 0.84	3.5	0.030	0.193	0.15	0.0042	

B1* 0.49	0.8	0.017	0.044	0.02	0.0159
B2* 0.54	0.8	0.021	0.044	0.02	0.0186
B3* 0.70	0.8	0.026	0.044	0.03	0.0212
B4* 0.75	0.8	0.030	0.044	0.03	0.0239

* Average of 2 repetitions.

The different τ^* levels for the low and high relative submergence scenarios, were achieved by adjusting the flume bed slope, S, because the flow depth, H, was kept constant for each scenario. Uniform flow conditions along the complete flume length were ensured via a set of rods placed one on top of the other along the flume width at the exit of the flume and by accordingly adjusting the volumetric flow rate, Q.

Each τ^* level corresponded to a predetermined multiple of the critical dimensionless shear stress (τ^*_{cr}) for incipient motion of the entrainable material. The concept of the probability of entrainment was adopted as the incipient motion criterion for this study, and the probability of incipient motion was set equal to 2% (Papanicolaou et al. 1999), which corresponds to an isolated particle. The critical bed shear stress was determined via image analysis of the particle incipient motion to be τ^*_{cr} = 0.0085. The entrainable material consisted of a glass, spherical particle mixture with diameters 8 mm, 15.9 mm, 19.1 mm, 22.2 mm and 25.4 mm, respectively. The fraction of each size in the mixture was determined such that the mixture grain size distribution matched the one from Oak Creek (Diplas 1987). The particles of size were of different color to facilitate their identification in the images. The dimensionless bedload feed rate at each τ^* level was determined from a recalibrated version of the Paintal (1971) formula against the data from Strom et al. (2004) as:

$$q_s^* = \frac{q_s}{\rho_s \cdot \left[g \cdot \left(\frac{\gamma_s}{\gamma} - 1 \right) \cdot d_{50}^3 \right]^{0.5}} = 0.0996 \cdot \left(\tau^* \right)^2 \qquad (2)$$

where q_s^* = dimensionless bedload rate, q_s = bedload rate, ρ and ρ_s = density of the fluid and the sediment, respectively. The bedload rate was determined by drying and weighing the sediment captured at a sediment trap placed at the exit section of the flume over a time interval of 5 minutes. The measured sediment mass was divided by the 5 minute sampling time interval and the flume width to calculate q_s.

2.2 *Flume Setup and Instrumentation*

The experiments were carried out in a 21 m long, 0.91 m wide and 0.53 m deep flume at the IIHR-Hydroscience and Engineering of the University of Iowa. The flume walls were made of acrylic glass that enabled side observations of the experiments. The test section was 5.2 m in length and was located 10.9 m from the flume entrance. A series of clast particles (d_c = 55 mm) were placed in a staggered arrangement and having $6d_c$ spacing between them atop a flat immobile bed that consisted of three layers of well-packed spherical glass particles with diameter d_b =19.1 mm. (Figure 3a). A 5.8 m long section upstream of the test section was used as bedload feed section, which permitted the bedload to enter the clast section by entrainment by the flow rather than manual feed.

Flow measurements in the test section were acquired via a two component Acoustic Doppler Velocimeter (ADV) and via the Large Scale Particle Image Velocimetry (LSPIV) technique. The ADV was utilized to take point measurements of the streamwise and vertical velocity components at 40 locations around a representative clast (Figure 3b). At each location, the ADV measurements were taken at 15 points at different depths resulting to a total 600 ADV measurements (Figure 3b). The sampling period for each ADV measurement was chosen to be 2 minutes. The ADV measurements were feasible only for the HRS runs. LSPIV measurements were also performed to resolve the velocity distribution at the water surface for both HRS and LRS runs but without the presence of the clasts. The LSPIV technique relies on recording the movement of tracer particles seeded on the water surface and subsequently trace the movement of these particles for producing velocity vectors. The tracer particles were 2 mm in diameter, Styrofoam particles that were seeded 0.50 m upstream of the clast section. Their movement was recorded with a Canon ZR85 Digital Camcorder mounted above the observation area at a rate of 30 frames per second for a total of two minutes. The captured video was converted to a sequence of images, which were enhanced via the Photoshop software. The enhanced images were then supplied to the LSIV software, which analyzed each successive pair of images and produced an instantaneous surface velocity map. These maps were then averaged over the period of one minute.

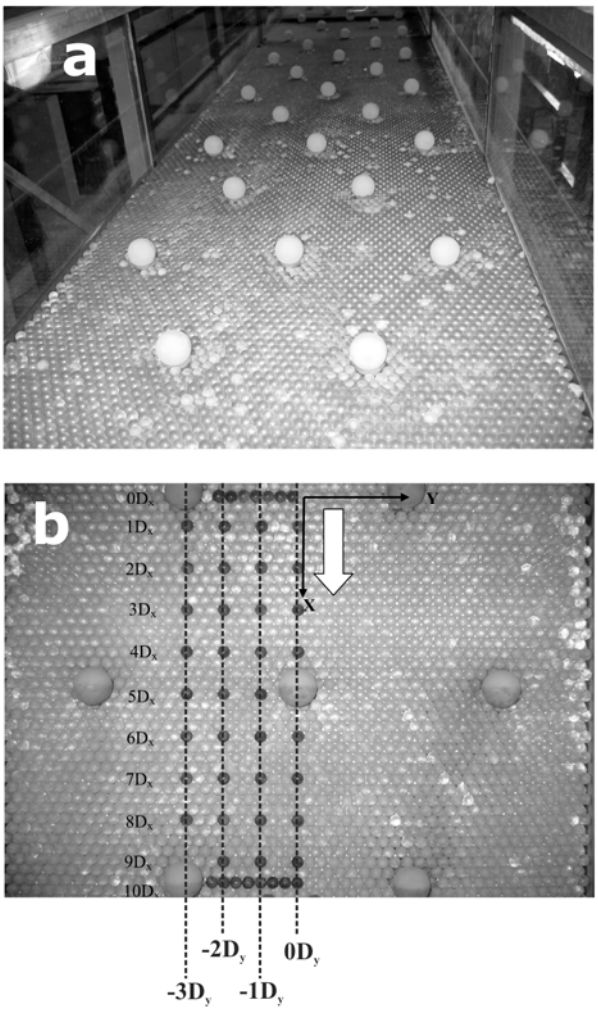

Figure 3. (a) Perspective view of the clast section and (b) ADV measurement transects.

3 RESULTS

3.1 *Flow Analysis Around Clasts*

Figures 4a and 4b show maps of the vertical streamwise velocity plane that were produced from the ADV profiles at transects $0D_y$ and $-3D_y$ (Figure 3), respectively for the HRS conditions. These figures indicate that as the flow approaches a clast, the flow separates and an upper and a lower layer appear along the flow depth. Fluid moving in the upper layer towards the free surface is minimally affected by the presence of the clast, whereas fluid of the upper layer close to the crest of the clast accelerates. In contrast, fluid in the lower layer decelerates and a recirculation region develops behind the clasts, where the streamwise velocity attains very small positive or even negative values. The recirculation region extends between $2d_c$-$4d_c$ downstream of the clast. A free shear layer develops at the interface of the upper and lower layers in the clast wake, extending from the crest of the clast and terminates at the point of the flow reattachment. Beyond the point of reattachement the flow continues to the next downstream clast, where the same pattern is observed (Figure 4b). These observations are in good agreement with the findings of previous researchers (Best et al. 2001; Shamloo et al. 2001).

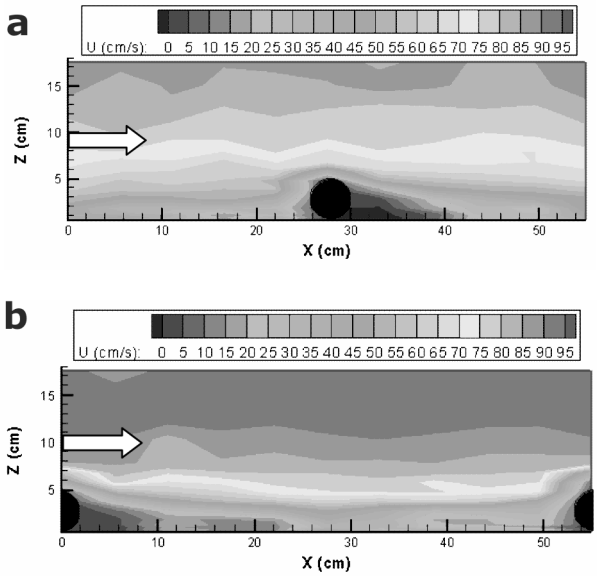

Figure 4. Streamwise velocity contours constructed from the ADV measurements for HRS for transects (a) $0D_y$ and (b) $-3D_y$.

A comparison of the streamwise velocity magnitude in transects $0D_y$ and $-3D_y$, (Figures 4a and 4b, respectively) reveals that the streamwise velocity magnitude increases at the outer transect $-3D_y$ (Figure 4b) comparatively to the middle transect $0D_y$ (Figure 4a). It is postulated that this increase is due to the presence of secondary currents in the flume transverse direction. The width/depth ratio of the flume is B/H =5.2, which is close to the upper threshold value where secondary currents become negligible (B/H =5.2) (Tamburino and Gulliver, 1999). However, the presence of the clasts amplifies the formation of the secondary currents in the adjacent region between the clasts. The secondary currents give rise to the formation of streamwise vortices in this adjacent region, which downwell close to the flume walls. This flow downwelling leads to the increased streamwise velocity magnitude of transect $-3D_y$ comparatively to transect $0D_y$.

Figure 5 illustrates a comparison of the measured velocity profiles at transect $-3D_y$ against the logarithmic law for rough boundaries (Kironoto and Graf, 1994). This comparison allows to evaluate the effects that the additional form roughness due to the presence of the clasts has on the flow. The measured velocity profiles are in good agreement with the logarithmic law at the outer layer, whereas a considerable deviation from the logarithmic law appears in the overlap layer. This deviation becomes more significant for the locations within the stagnation region behind the clast

and is the smallest for profile $5D_x$, which is located farthest away from the clasts. This deviation is attributed to the flow structures and more specifically to the horseshoe (HS) vortex (Shamloo et al. 2001) generated around the clast as the flow impinges on the clast and separates around it.

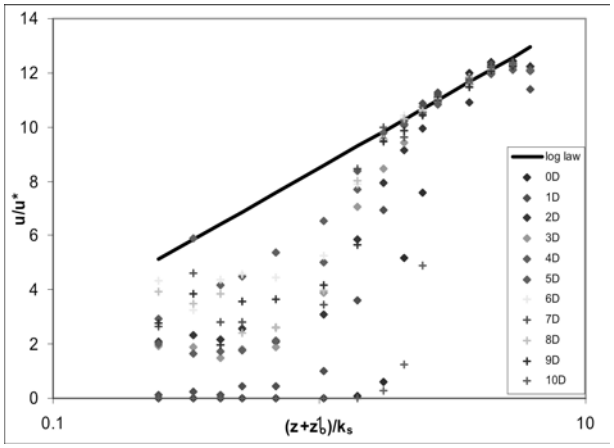

Figure 5. Comparison between the measured velocity profiles along transect $0D_y$ and the log law.

Furthermore, Figure 5 shows that at least 3 of the plotted 11 profiles (i.e. profiles $0D_x$ and $1D_x$) of transect $0D_y$ show that the streamwise velocity decreases close to the water free surface. This indicates that in the HRS regime, the presence of the clasts is barely felt in the free surface. This can also be verified from the water surface velocity maps produced by the one-minute average of the LSPIV measurements, shown in Figure 6a. The flow field for HRS conditions in Figure 6a is symmetric about the flume centerline and there is a gradual reduction of the surface velocity from the flume centerline towards the flume walls. The measurements from the LSPIV method are also in agreement with the ADV profiles.

In contrast, for LRS conditions, the surface velocity field consists of patches of low and high speed moving fluid (Figure 6b). This suggests that the effects of the bed surface roughness are well depicted at the free surface, which in turn indicates that the flow distribution at the free surface directly reflects the spatial distribution of the clasts.

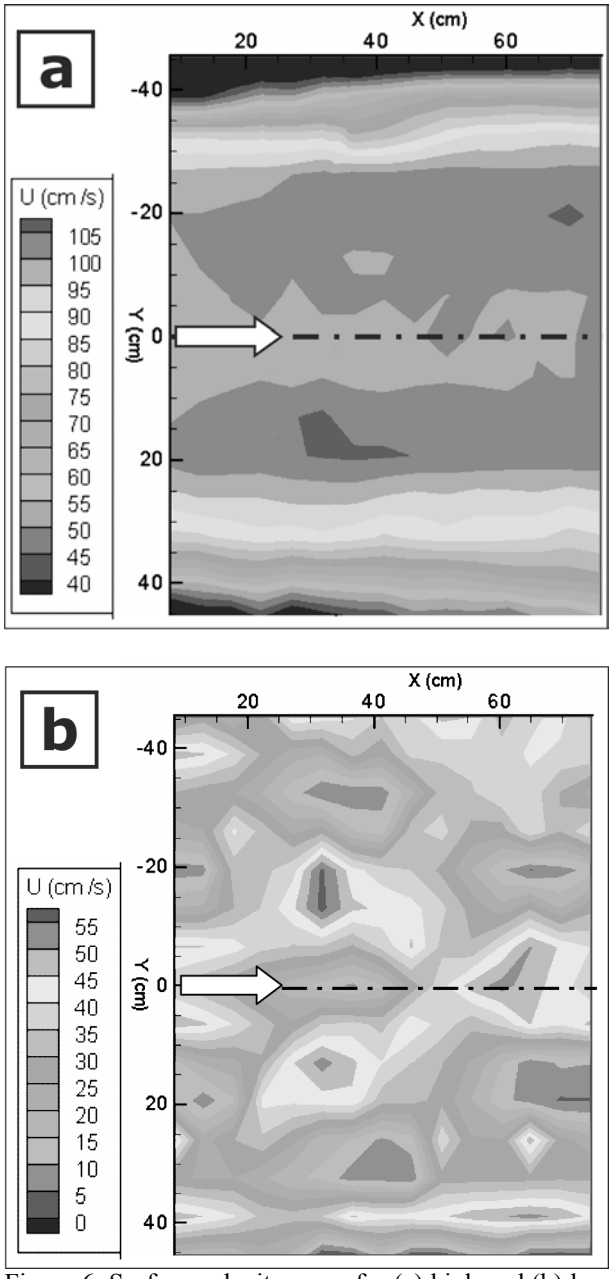

Figure 6. Surface velocity maps for (a) high and (b) low relative submergence conditions.

Figure 7 is a plot of the vorticity map at the water surface around a clast obtained by the LSPIV surface velocity measurements for the LRS regime. The vorticity map clearly highlights the limbs of the horseshoe vortex that develops around the clast. The two HS vortex limbs have vorticity of opposite sign, and thus act as a sweep in the clast wake region. The HS vortex extends approximately $3.5d_c$ downstream of the clast. The fact that the HS vortex can be captured by surface velocity measurements indicates that under LRS conditions, it occupies the complete flow depth. This finding further supports the fact that the patterns of the velocity at the water surface under LRS conditions are regulated by the presence of the clasts.

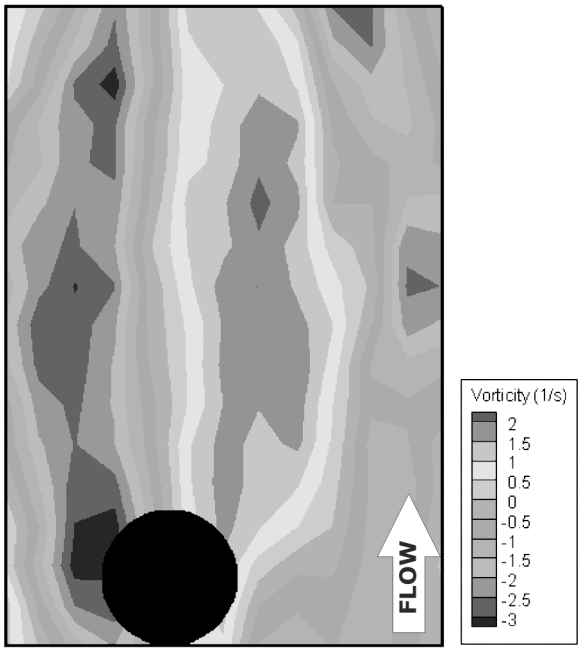

Figure 7. Surface vorticity maps around a clast for HRS conditions.

3.2 *Interaction Between Flow And Clasts*

Figure 8 shows an image of the LSPIV seeding material superimposed on an image of the flume bed topography during the LRS runs. The white patches in the image highlight the structure of the horseshoe vortex around each clast. The limbs of each horse vortex extend to the vicinity of a downstream clast. The incoming bedload particles deposit between the limbs of neighboring horseshoe vortices at the upstream face of the clasts. In contrast, no significant deposition is observed in the wake of the clasts, which is attributed to the presence of the HS vortex and its counter-rotating limbs. The latter indicates that the depositional patterns under LRS conditions are predominantly regulated by the flow structures (i.e. horseshoe vortices) developing around the clasts. Therefore, the sediment deposition patterns around the clasts are dictated by the clast geometry, which affects the flow patterns around the clasts.

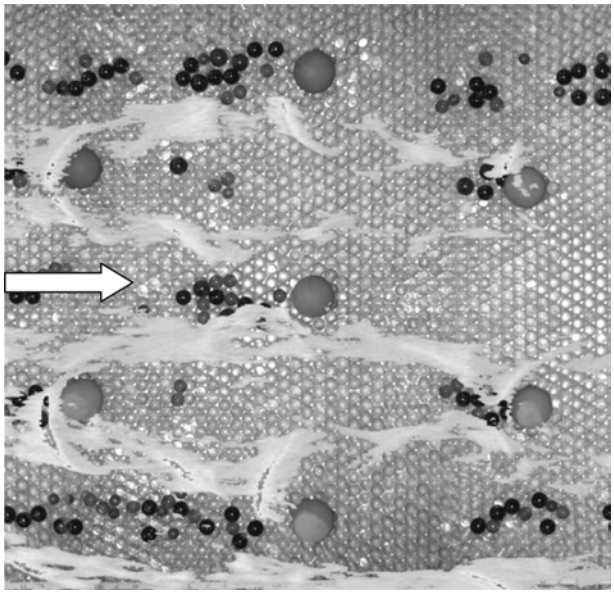

Figure 8. Superimposed LSPIV seeding material with the cluster depositional patterns.

Figures 9a and 9b show representative patterns of deposited bedload particles around a clast for the HRS and LRS regimes, respectively. Under the HRS regime, particles typically deposit at the downstream face of the clasts. This is attributed to the development of the stagnation region behind the clasts (Figure 4a), which offers sheltering to the incoming particles from the flow action. In contrast, under the LRS regime, particles accumulate at the upstream face of the clasts. Particles tend to be deposited at same locations as the crests of the waves that form due to the presence of the clasts (Figure 9b). This observation further supports the argument that clasts dictate the depositional patterns of incoming sediment under the LRS regime.

4 CONCLUSIONS

This research presented an experimental investigation of the role of relative submergence on the interaction between rocks and the surrounding flow and association of this interaction to the depositional patterns of incoming sediment around the rocks. A series of experiments were conducted for each of these two flow regimes. Velocity measurements were collected at the vicinity of the clasts via Acoustic Doppler Velocimetry (ADV) and Large Scale Particle Image Velocimtery (LSPIV). The main finding of this study was that different flow structures develop around the clasts for high and low relative submergence. For high relative submergence, a stagnation region developed behind the clasts but their presence was not reflected in the free surface. Instead, for low relative submergence, the presence of the clast was felt at the water free surface and a horseshoe vortex with counter-rotating limbs developed around

the clasts. The sediment deposition patterns around the rocks were different under high and low relative submergence regimes and were dictated by the flow structures generated due to the clast presence. Under HRS the incoming sediment deposited predominantly within the stagnation region of the clast. Instead, for LRS conditions incoming sediment accumulates in the stoss region of the clast. The findings from this study are the first step for an improved understanding of the hydraulics of these rock structures, which will contribute to the establishment of a mechanistic approach for the design and placement of rock structures in mountainous streams.

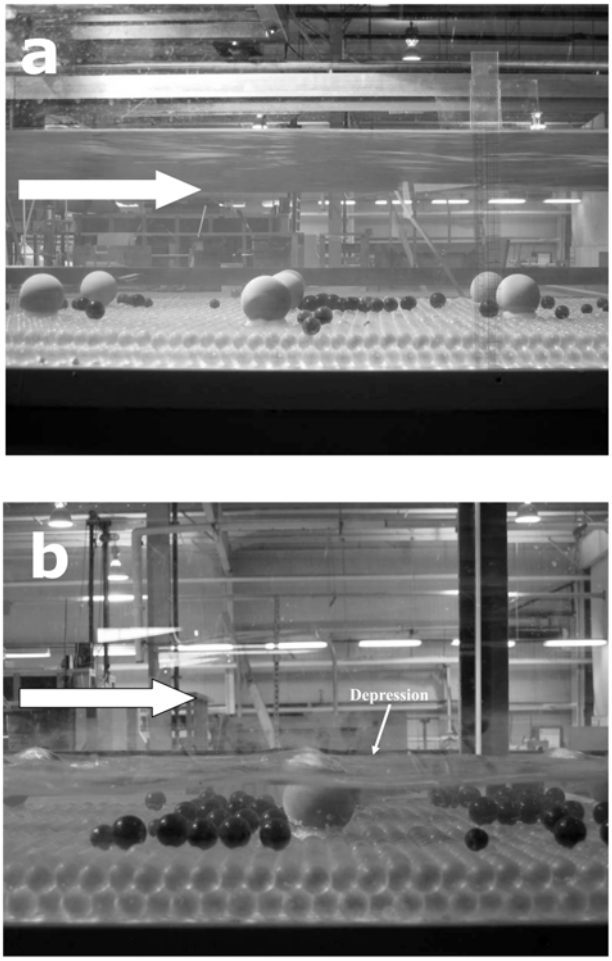

Figure 9. Depositional geometry of incoming sediment under (a) high and (b) low relative submergence conditions.

REFERENCES

Best, J.L., Buffin-Belanger, T., Kirkbride, A.D., Reid, I. 2001. Visualization of coherent flow structures associated with particle clusters: temporal and spatial characterisation revealed using ultrasonic Doppler velocity profiling, In: Nolan, T.J., Thorne, C.R. (Eds) Gravel Bed Rivers 2000, Special Publication of the New Zealand Hydrological Society.

Bettess, R. 1984. Initiation of sediment transport in gravel streams. Proceedings of the Institute of Civil Engineers, 77(2), 79-88.

Diplas, P. 1987. Bedload Transport in gravel-bed streams. Journal of Hydraulic Engineering, 113(3), 277-292.

Fischenich, C., Seal, R. 2000. Boulder Clusters. EMRRP Technical Notes Collection (ERDC TN-EMRRP-Sr-11) U.S. Army Engineer Research and Development Center, Vicksburg, MS, www.wes.army.mil/el/emrrp.

Kironoto, B.A., Graf, W.H. 1994. Turbulence characteristics in rough uniform open-channel flow. Proceedings of the Institute of Civil Engineers, Watershed and Maritime Energy, 106, 333-344.

Paintal, A.S. 1971. A stochastic model of bedload transport. Journal of Hydraulic Research, 9(4), 527-554.

Papanicolaou, A.N., Diplas, P., Bala, M., & Dancey, C.L. 1999. Computer vision technique for tracking bed load movement. Journal of Computing in Civil Engineering, 13, 71 - 79.

Saldi-Caromile, K., Bates, K., Skidmore, P., Barenti, J., Pineo, D. 2004. Stream habitat restoration guidelines: Final draft. Co-published by the Washington Departments of Fish and Wildlife Ecology and the U.S. Fish and Wildlife Service. Olympia, Washington.

Shamloo, H., Rajartnam, N. & Katopodis, C. 2001. Hydraulics of simple habitat structures. Journal of Hydraulic Research, 39(4), 351-366.

Strom, K., Papanicolaou, A.N., Evangelopoulos, N. & Odeh, M. 2004. Microforms in gravel bed rivers: formation, disintegration and effects on bedload transport. Journal of Hydraulic Engineering,130(6), 554-567.

Tamburino, A., Gulliver, J.S. 1999. Large flow structures in a turbulent open channel flow. Journal of Hydraulics